DOI: https://doi.org/10.37434/tpwj2026.10.01

AUTOMATED DETECTION OF DEFECTIVE AREAS IN A MULTILAYER THIN-WALLED STRUCTURE WITH A PERIODIC CONFIGURATION USING LASER INTERFEROMETRY METHODS

L.M. Lobanov, I.L. Shkurat, O.P. Shutkevych, I.V. Kyianets, V.V. Savitsky

E.O. Paton Electric Welding Institute of the NASU
11 Kazymyr Malevych Str., 03150, Kyiv, Ukraine

ABSTRACT

Simulation and data analysis methods were applied to detect and evaluate deformations in thin-walled structures with a periodic configuration, particularly in welded multilayer panels. The use of the finite element method made it possible to determine characteristic spatial deformation profiles and their relationship to defect localization. Fourier analysis and differentiation techniques were used to develop an algorithm for the automated detection of defective areas in thin-walled structures. It is shown that the use of the displacement derivative $\partial w/\partial y$ provides more precise localization of defects compared to an analysis of displacements alone. This justifies the feasibility of applying the shearography method as one of the most informative approaches to the non-destructive testing of such structures. The obtained results are confirmed by both numerical and experimental data, indicating the suitability of the methodology for diagnosing a wide class of thin-walled structures.

KEYWORDS: thin-walled structures, stress-strain state, finite element method, Fourier analysis, non-destructive testing, laser interferometry, shearography, automated defect detection

INTRODUCTION

Metal multilayer thin-walled panel-type structures (welded panels) are widely used in aircraft manufacturing, automotive manufacturing, shipbuilding, and other sectors of mechanical engineering. Such structures are characterized by high specific strength and stiffness at a low mass, which is achieved through the rational distribution of material among the layers and elements of the panel. In addition, the panel structure ensures the manufacturability of large-sized elements with complex shapes and enables the localized reinforcement of the most heavily loaded areas without a significant increase in the total mass of the product [1, 2].

One of the most common methods for joining the components of such structures is spot welding, which is distinguished by high efficiency and ease of automation. The use of spot welding allows for the production of metal structures with high strength and minimal residual distortion compared to structures made with continuous welds [3].

Because of the specific nature of spot welding (a brief process, localized heating, and rapid cooling), this type of joint is highly prone to hidden defects. In particular, defects such as lack of fusion, weld nugget failure, and delamination may form; they significantly reduce the operational reliability of the structure.

Since such defects cannot be detected during visual inspection, and their presence directly affects the operational reliability of the structure, the use of various non-destructive testing methods for the timely detection of defects becomes particularly important [4–7].

Copyright © The Author(s)

Among the conventional approaches to inspecting spot welds, ultrasonic, eddy current, X-ray, and other non-destructive testing methods are used [8–10]. However, their use in inspecting large-scale panel structures with a large number of spot welds has limited efficiency, due to the need to inspect individual welded joints sequentially.

Among the existing methods of non-destructive testing, some of the most effective are laser interferometry methods, in particular holographic interferometry, speckle interferometry, and shearography [11–14]. These methods are based on recording and subsequent analysis of data on the deformation of areas of the surface of the object under study, which occurs under the action of an external load. Due to their high sensitivity to local changes in the stress-strain state, these methods enable the detection of hidden defects that are difficult to detect using conventional (contact) inspection methods. The non-contact nature and high spatial resolution of these methods make it possible to obtain full-field maps of surface deformations and enable automated inspection of thin-walled structures.

Despite the high informativeness and sensitivity of laser interferometry methods, the analysis of the obtained results is, in most cases, performed manually by an operator. This reduces the efficiency of the inspection and increases the dependence of diagnostic results on the specialist's skills and subjective experience [11–14]. This is particularly true for the inspection of complex-shaped structures or structures with a periodic configuration, where local changes in the strain field may be poorly noticeable against the back-

ground of the overall distribution of displacements, making it difficult to reliably determine the location of a defective area based on the results of a visual analysis of the object's surface strain field.

In this regard, it is important to develop a method for the automatic detection and localization of defects in thin-walled structures during non-destructive testing using optical methods. Implementing such an approach will reduce the subjective influence of the operator and improve the accuracy of defect localization. Existing approaches to automated defect detection in regular three-dimensional structures are based on mathematical simulation and the solution of optimization problems involving structural parameters [15]. In contrast to these methods, this paper proposes an algorithm for the automated detection of defective areas in structures with a periodic configuration based the Fourier analysis of the surface deformation profile obtained from shearography testing, the generation of a reference defect-free segment, and the calculation of a quantitative assessment of the deviation of the deformation profile.

NUMERICAL SIMULATION OF THE STRESS-STRAIN STATE OF A WELDED PANEL USING THE FINITE ELEMENT METHOD

The finite element method was used to model the stress-strain state (SSS) that arises during non-destructive testing under various types of loading. A two-layer welded structure consisting of a face sheet and a corrugated core of trapezoidal profile joined by spot welding was selected as the object of study. The core has a periodic shape: its rectilinear segments alternately contact the upper face sheet and a hypothetical plane of the lower face sheet. The panel, measuring 800×600×50 mm, is made of 2 mm thick St3 steel; the diameter of the weld spots is ~6 mm. A three-dimensional model was constructed, and used for numerical simulation of the SSS by the finite element method (Figure 1).

The problem was solved in a three-dimensional formulation within the framework of weakly coupled linear thermoelasticity, without taking plastic deformations into account and without considering the temperature dependence of material properties. In the first stage, the temperature distribution $T(x, y, z, t)$ was determined from the heat conduction equation $\rho c \cdot \partial T/\partial t = \mathrm{div}(\lambda \cdot \mathrm{grad} T)$ with a heat flux applied to one side of the panel (a second-kind (Neumann) boundary condition) and an initial temperature corresponding to room temperature ($T_0 \approx 293$ K). The resulting temperature field was used as the thermal load in the elastic equilibrium problem $\mathrm{div}(\sigma) = 0$, where σ is the stress tensor. Stresses were determined using Hooke's law for a linearly elastic isotropic material, taking into account thermal strain (in the simplified uniaxial form): $\sigma = E(\varepsilon - \alpha \Delta T)$, where ε is the total strain, α is the coefficient of linear thermal expansion, and $\Delta T = T - T_0$ is the change in temperature relative to the initial state.

The panel material (St3 steel) was modeled as a linearly elastic isotropic material with the following properties: modulus of elasticity E = 200 GPa, Poisson's ratio $\nu = 0.3$, coefficient of linear thermal expansion $\alpha = 12 \cdot 10^{-6}$ 1/°C, thermal conductivity $\lambda = 50$ W/(m·K), specific heat capacity $c = 470$ J/(kg·K), and density $\rho = 7850$ kg/m^3. The coefficients E and ν determine the elastic properties of the material in the three-dimensional formulation of the problem.

The boundary conditions were specified separately for the mechanical and thermal parts of the problem. In the areas of the core that, in the complete structure, are in contact with the lower face sheet (to simplify the model, the latter was excluded from the computational domain), the following conditions were imposed: a mechanical condition of full fixation ($u = v = w = 0$), which models the support provided by the lower face sheet; a first-order (Dirichlet) thermal boundary condition with a constant temperature $T = T_0$ (room temperature), which models the lower lining as a heat sink. Additionally, the side faces were fixed in the direction of the *OY* axis. A thermal load in the form of a heat flux was applied to the outer surface of the upper face sheet; the remaining surfaces of the structure were considered thermally insulated.

The SALOME software [16] was used to generate the finite element mesh, and the thermal and stress-strain analyses were performed using the Code_Aster software

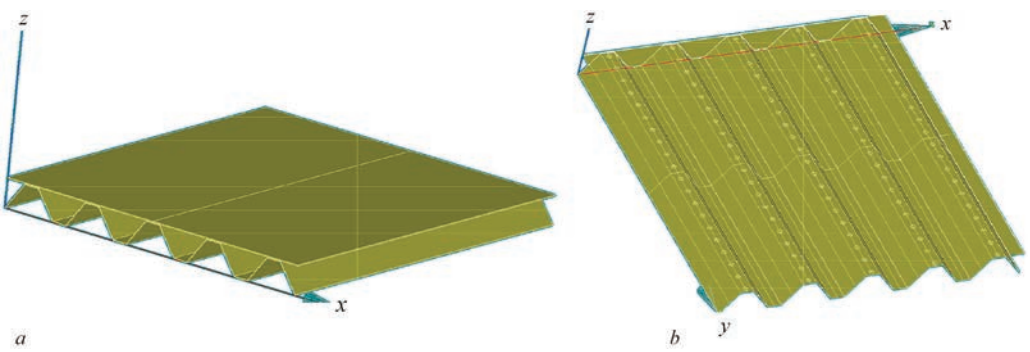


Figure 1. Geometric model of a welded structure: *a* — front view; *b* — view from the corrugated core side

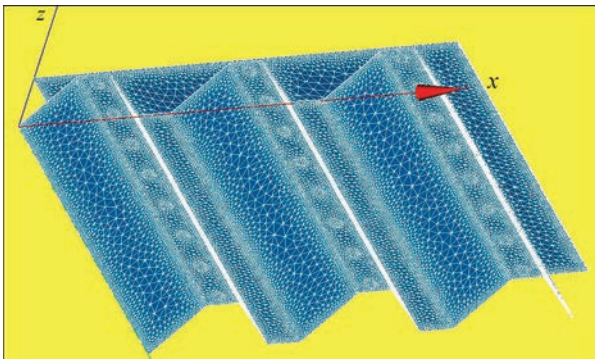


Figure 2. Finite element mesh of a simplified model of a welded panel

package [17]. The structure was divided into elements to form a three-dimensional tetrahedral mesh (Figure 2). The size of the mesh elements varied across the volume of the structure: the base discretization step was 0.5 mm, while in the areas of weld spots, where changes in surface curvature and joint geometry occur, the algorithm automatically generated a denser mesh with smaller elements compared to the rest of the structure.

The thermal load was simulated by heating the upper surface of the welded structure with a heat flux of Q_0 = 8000 W/m² for t_0 = 10 s. The distribution of temperature changes developing in the structure as a result of this thermal load is shown in Figure 3, where a local minimum in temperature changes is observed in the vicinity of the weld spots. This is explained by the presence of weld nuggets, which have higher thermal conductivity compared to the adjacent areas of the structure and ensure more intensive heat removal. Such unevenness in the temperature field leads to uneven deformation of the welded panel surface.

A simulation was performed to determine the distribution of w values (the normal displacement at points on the structure surface). Along cross-section 1, no significant local maxima are observed that could be used to assess the presence and diameter of weld spot nuggets (Figure 4).

The profile of the $w(y)$ component, plotted from displacement data along cross-section 1, makes it possible to determine the locations of weld spots; however, the amplitude of deformation disturbances around

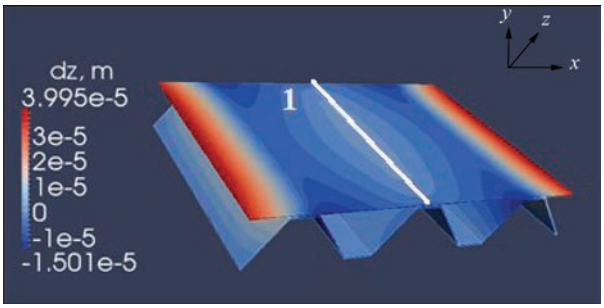


Figure 4. Distribution of displacements in a panel without welding defects

them varies, which makes it impossible to estimate the diameter of the nugget of an individual weld spot.

Figure 5 shows the distribution of $\partial w/\partial y$ (the derivative of w displacement with respect to the y coordinate along the cross-section of the structure under study), in which the coordinates of the weld spots are more clearly visible compared to Figure 4. Thus, for this type of structure, the use of the shearography method, which performs optical differentiation of the displacement field, is more appropriate than methods such as speckle correlation, speckle interferometry, and holographic interferometry. Analysis of this distribution makes it possible to assess the influence of each weld spot on the overall strain field of the outer surface of the structure. However, this configuration allows only a qualitative assessment of the defectiveness of a particular weld spot.

More informative is the curve showing the variation of the derivative $\partial w/\partial y$ plotted along cross-section *1*, which passes through the centers of the weld spots. Analysis of this dependence makes it possible to determine their locations. However, the amplitude of local deformation disturbances in the vicinity of individual spots varies, which complicates the estimation of the nugget diameter of an individual weld spot. Figure 6 shows the distribution of the displacement component w and its derivative $\partial w/\partial y$ along this cross-section. Analysis of the obtained dependencies shows that the centers of the weld spot nuggets appear as local minima. The diagram consists of repeating segments that correspond to the geometric parts of the structure. Unlike the displacement component w, for which a significant edge effect is observed, the distri-

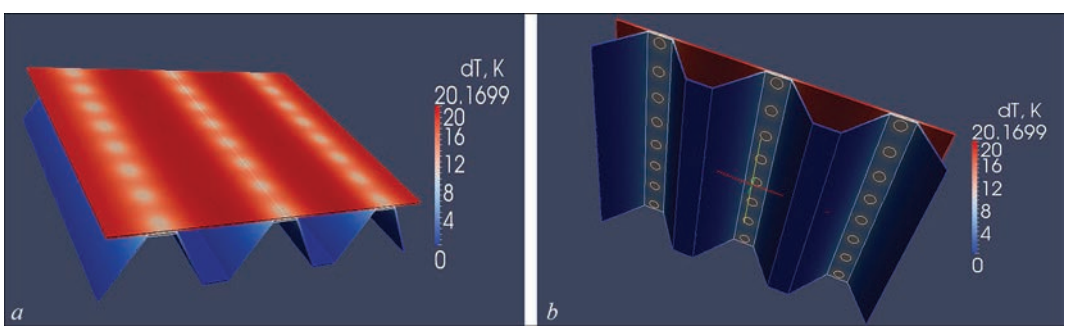


Figure 3. Distribution of temperature changes in the structure resulting from thermal loading: *a* — front view; *b* — view from the corrugated core side

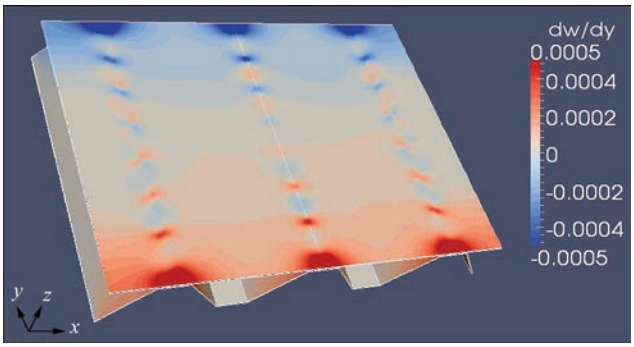


Figure 5. Distribution of the displacement derivative at surface points on a welded panel under thermal loading

bution of the derivative $\partial w/\partial y$ is more uniform. The edge effect changes the deformation pattern in the areas near the beginning and end of the structure.

A simulation was conducted to investigate the effect of the weld spot nugget diameter on the displacement w and its derivative in a welded panel along a selected direction y under thermal loading. To this end, defective weld spots lacking a high-quality joint were introduced, and their effect on the deformation of the object's surface was investigated (Figure 7).

Simulations have shown that, as a result of the thermal load on the structure, which was applied in a way similar to the experiments conducted during shearography testing, a complex deformation pattern emerges. Moreover, the amplitudes of w and $\partial w/\partial y$ at defective spots do not exceed those at neighboring spots. This fact complicates the process of defect detection and also necessitates the involvement of a highly qualified operator during non-destructive testing.

METHODOLOGY FOR THE AUTOMATED DETERMINATION OF DEFECT LOCATIONS BASED ON SURFACE DEFORMATION DATA UNDER STRUCTURE LOADING

The main objective of the developed algorithm is the automated determination of the locations of structure segments where the deformation differs significantly from the average deformation of areas in the profile.

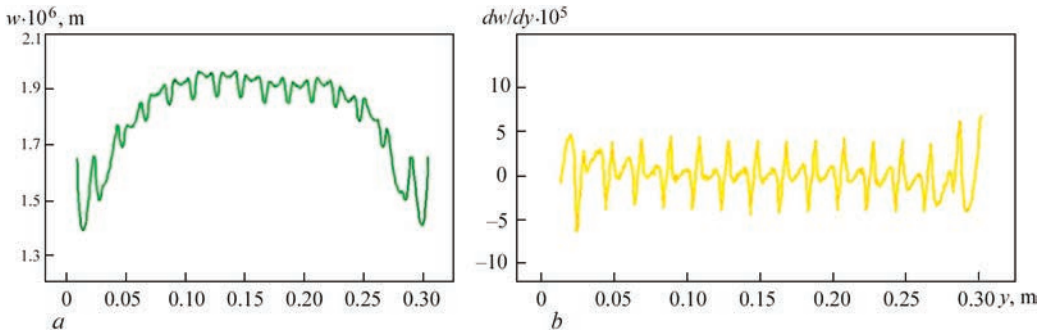


Figure 6. Distribution of displacements w (*a*) and its derivative $\partial w/\partial y$ along cross-section *1* under thermal loading of a two-layer panel

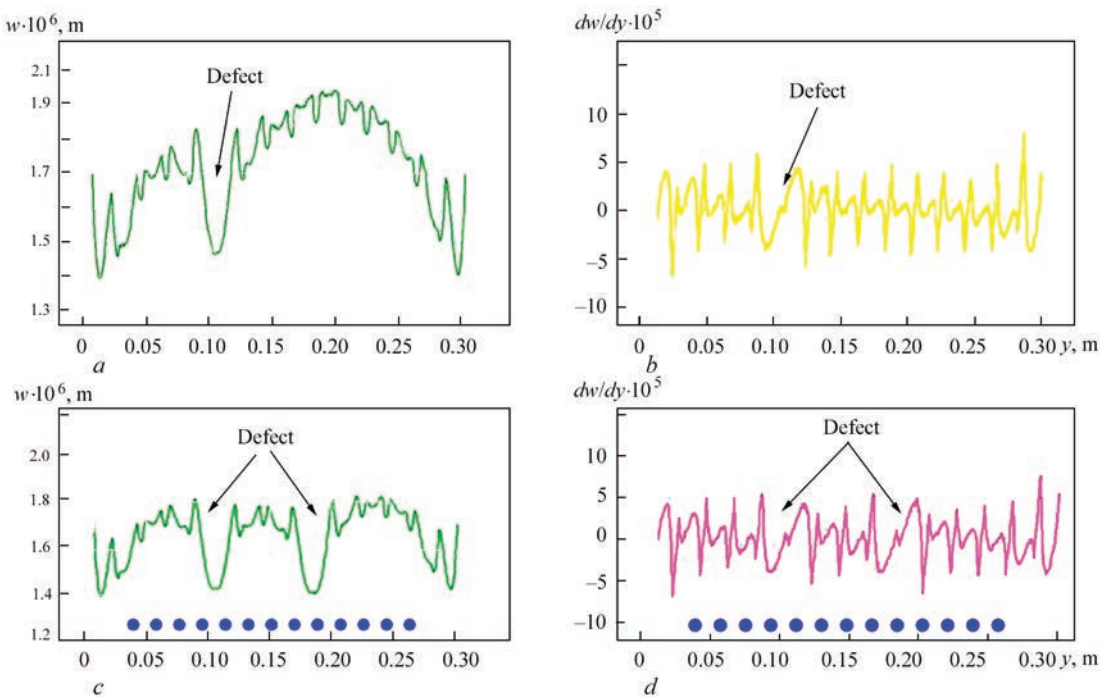


Figure 7. Dependences of the displacement w and its derivative $\partial w/\partial y$ in a welded panel with one (*a*, *b*) and two defective weld spots (*c*, *d*). The positions of the weld spots are marked in blue

Since the deformation P of the surface of the object under study of the object under study has a periodic configuration, it is rational to use the Discrete Fourier Transform (DFT) to determine its period. This is one of the fundamental methods widely used in digital signal processing algorithms [18], as well as in other fields related to the analysis of frequencies in discrete signals.

As a result of the Fourier transform, data can be obtained on the number of repeating segments N (the number of periodic segments included in the profile). Knowing the total length of the profile l under study and the total number of discrete points N_0 of the profile, the period T of the structural inhomogeneities and the number of points N_1 per one period T can be determined.

After dividing the profile into segments of length T, a reference defect-free segment of the profile P_{ref} is determined using averaging or a median filtering algorithm. The values of the components of the displacement vector along P_{ref} are calculated based on the assumption that the number of defective weld spots in the structure is small compared to their total number.

When averaging, all points $i = 1 - N_1$ in each segment of the profile (Figure 8) are taken into account, and the average value of the function at these points is calculated. This value corresponds to the value of the function at the i-th point of the reference defect-free segment.

A second method that can be used to obtain a reference defect-free segment is median filtering. Median filters are often used in practice as a means of preprocessing digital data [19]. A specific feature of the filter is its pronounced selectivity toward array elements that stand out sharply against the background of neighboring readings. At the same time, the median filter has no effect on the monotonic component of the sequence, leaving it unchanged. Due to this property, median filters with an optimally selected aperture can, for example, preserve the sharp edges of objects without distortion while effectively suppressing uncorrelated or weakly correlated noise and fine details. This property allows median filtering to be used to remove anomalous values in data arrays and reduce impulse noise.

For odd n, the median of a numerical sequence x_1, x_2, … , x_n and, for an odd n, is the value in the middle of the sequence sorted in ascending (or descending) order. For even n, the median is usually determined as the arithmetic mean of the two middle values of the ordered sequence.

A median filter is a window filter that sequentially slides across a data array and, at each step, the median of the elements within that window. The output signal y_k of a median filter with an aperture $2n + 1$ for the current sample k is formed from the input time series according to the formula:

$$y_k = \text{med}(x_{k-n}, x_{k-n+1}, \dots, x_{k-1}, x_k, x_{k+1}, \dots, x_{k+n-1}, x_{k+n}), \quad (1)$$

where $\text{med}(x_1, \dots, x_m, \dots, x_{2n+1}) = x_{(n+1)}$, x_m are elements of the variational series, i.e., ordered in ascending order of the values x_m: $x_{(1)} = \min(x_1, x_2, \dots, x_{2n+1}) \le \le x_{(2)} \le x_{(3)} \le \dots \le x_{(2n+1)} = \max(x_1, x_2, \dots, x_{2n+1})$.

A median filter was used as follows: for each segment of the profile, the points $i = 1 \dots N_1$ with deformation data were selected; the function values at these points were sorted in ascending order; from N_1 values, the value at position $(N_1+1)/2$ was selected for odd N_1, or the average of the values at positions $N_1/2$ and $N_1/2+1$ for even N_1. In this way, abnormally small and large function values were filtered out.

Determining a reference defect-free segment from real data can be somewhat complex. To obtain this segment during simulation, it is sufficient to construct a defect-free structure and average all profiles of the desired type. When processing real data, it is impossible to guarantee in advance that a structure will be defect-free or to select a direction, whose profile will be defect-free. Therefore, to obtain a reference defect-free segment, the data from all suitable profiles should be averaged.

After obtaining a reference defect-free deformation profile P_{ref}, it is necessary to compare it with all segments of the selected cross-section and determine the maximum deviations of the measured deformation values from the reference profile data. To determine the extent to which the deformation profile P differs from the displacement values of the reference segments, a function was introduced to calculate the deviation of the deformation of the segments P_n from the reference area P_{ref}:

$$D(n) = \frac{\sum_{i=1}^{N_1} \left| P_{ref}^i - P_n^i \right|}{N_1}, \quad (2)$$

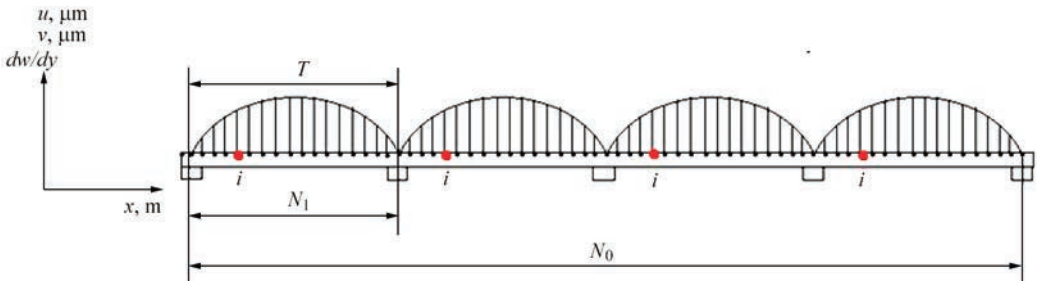


Figure 8. Periodic structure of the deformation profile with an example of point selection for averaging

where n is the segments number, N_1 is the total number of points in the selected segments with displacement data, P^i_{ref} is the displacement value at the point with index i of the reference profile, and P^i_n is the displacement value at the point with index i of the selected segments of the profile P.

The following algorithm was developed to detect areas of the structure with defects:

1. The period T of structural inhomogeneities in the object under study is determined based on data from the deformation profile P of its surface along the length l, as well as the number of points N_1 of the discrete function describing the displacement or the displacement derivative within one period.

2. The deformation profile P is divided into segments P_n, each of length T.

3. The profile of the reference defect-free segment P_{ref} is calculated based on deformation data for individual segments P_n (average or median values are calculated).

4. A diagram $D(n)$ is plotted showing the deviation of the deformation in the segment P_n from the reference defect-free segment P_{ref}.

5. Based on the analysis, the locations of the defective areas are determined by the maximum values of the function $D(n)$.

The proposed algorithm was tested on characteristic deformation profiles of the surface of a two-layer welded panel.

Unlike the conventional approach, in which the operator concludes that a defect is present based on a visual analysis of the deformation pattern, the function $D(n)$ makes it possible to establish a quantitative criterion for the presence of a defect. An segment P_n is considered defective if the condition $D(n) > D_{thr}$ is satisfied, where the threshold value D_{thr} is determined based on the statistical characteristics of the distribution of $D(n)$, for example, $D_{thr} = D_m + k\sigma_D$, where D_m and σ_D are the mean and standard deviation of the function $D(n)$ throughout all segments of the profile, and k is a coefficient that determines the sensitivity of the inspection. The use of this criterion reduces the subjective influence of the operator on the results of non-destructive testing.

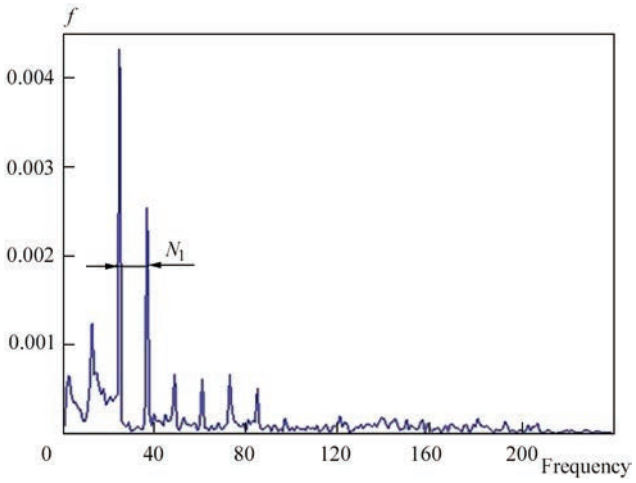


Figure 9. Fourier spectrum of the profile $\partial w/\partial y$ along a selected cross-section: the step between peaks (equal to N) determines the number of points N_1 per profile period, $N_1 = N_0/N$

ANALYSIS OF THE DEFORMATION PROFILE OF THE SURFACE OF A WELDED PANEL WITH DEFECTS

To determine the location of defects in a welded panel, the distributions of the displacement w and its derivative $\partial w/\partial y$ along cross-section 1 under thermal loading of a two-layer panel were analyzed. The deformation profiles under study are characterized by a significant number of local maxima and minima; however, the amplitude of deformation in the vicinity of defective areas does not exceed the amplitude of deformation in defect-free areas. This complicates the direct detection of defects based on the analysis of deformation profiles.

To determine the principal period, a Fourier transform was performed on the profile $\partial w/\partial y$ along the selected cross-section (Figure 9). The obtained spatial spectrum is characterized by sharp maxima, the abscissa axis shows the spatial harmonic number (frequency), and the ordinate axis shows the amplitude.

The obtained diagram shows sharp peaks maxima, the distance between which corresponds to the number of segments N in the structure. In this welded panel, $N = 12$. Since the total number of points is $N_0 = 480$, there are 40 points per segment. If it is impossible to determine the period from the first harmonic because it is obscured by low-frequency noise, the second or subsequent harmonics are used, and the distance between them is determined. The reference profile $\partial w/\partial y$ of a defect-free segment was generated using three different methods (Figure 10), but they do not differ significantly.

Figure 11 shows the distribution of deviations $D(n)$, where the x-axis is labeled with the segment number n. Analysis of the distribution shows that in

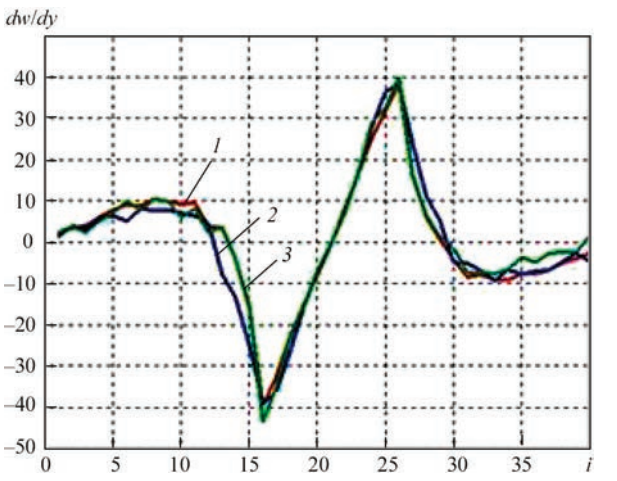


Figure 10. Reference profile ∂w/∂y for a defect-free segment, obtained by averaging the defect-free profile (*1*), averaging the defective profile (*2*), and applying median filtering (*3*), where i is the ordinal number of a discrete point within a single period of the structure profile

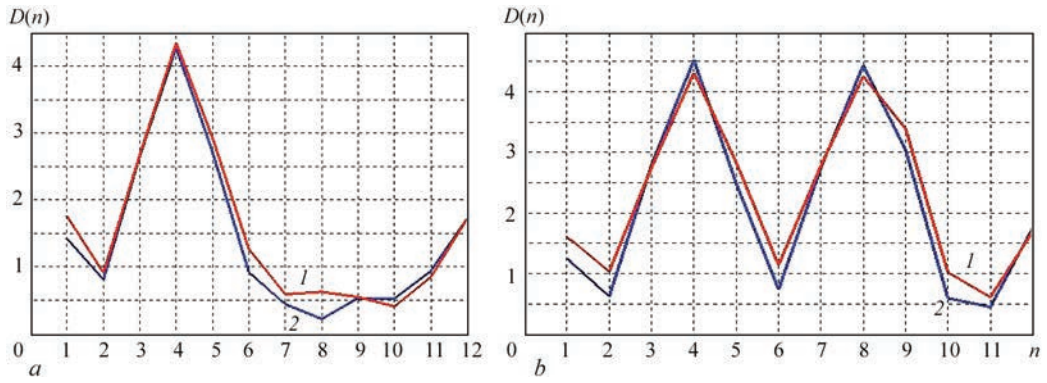


Figure 11. Dependence of $D(n)$ on the segment number n: *1* — based on averaging data; *2* — based on median filtering data

the first case, the defect is localized in the 4th segment (Figure 11, *a*), and in the second case, in the 4th and 8th segments (Figure 11, *b*).

The data obtained using simple averaging and median filtering do not differ significantly. However, the $D(n)$ functions calculated using median filtering have lower values in defect-free segments. Therefore, median filtering provides more accurate results. The developed algorithm demonstrated high efficiency in determining the location of a defect in a welded panel.

DETECTION OF DEFECTS IN A THREE-LAYER WELDED PANEL DURING ITS NON-DESTRUCTIVE TESTING USING THE SHEAROGRAPHY METHOD

The developed algorithms were tested on a three-layer welded panel. The experimental specimen differs from the model problem discussed above in geometry, materials, and type of loading, which makes it possible to assess the versatility of the proposed approach for structures with a periodic configuration. The study utilized non-destructive testing data obtained using the shearography method on a panel measuring 190×110×5 mm; the load-carrying layers were made of 03Kh11N10M2T steel with a thickness of 0.6 mm, while the joining material was made of 0.3 mm thick 12Kh18N10T steel.

The mechanical load was performed by introducing a volume of air V = 5 cm^3 into the center of the panel through a side opening. As a result of shearography testing, an image of the distribution of the displacement derivative $\partial w/\partial y$ (Figure 12) was obtained as a grayscale image: the darkest areas correspond to the smallest values, and the lightest areas to the largest.

For further investigation, profiles *1* and *2* (defect-free) and profile *3* (passing through the zone of influence of a defect) were selected from the structure. The defect in the structure is a fractured spot weld between the face sheet and the core. To reduce speckle noise, the deformation image was processed using Gaussian filtering. This filter does not change the period of the characteristic deformation features and, therefore, does not affect the results of the automatic determination of the period T.

To determine the location of a defect in a weld spot (lack of fusion), the experimental data on the derivative of the displacement component $\partial w/\partial y$ were processed using the same algorithm as the model data. During data processing, a diagram of the derivative distribution (Figure 13, *a*) was plotted along profile 1; the influence of a defect on this profile is not evident. The dimensionless quantity I, determined by the shearography method and representing a characteristic of the object deformation, is plotted on the y-axis. The Fourier spectrum (Figure 13, *b*) shows a distinct maximum corresponding to the number of periodic segments of the structure included in the profile (N = 9); there are N_1 = 51 points per a typical panel

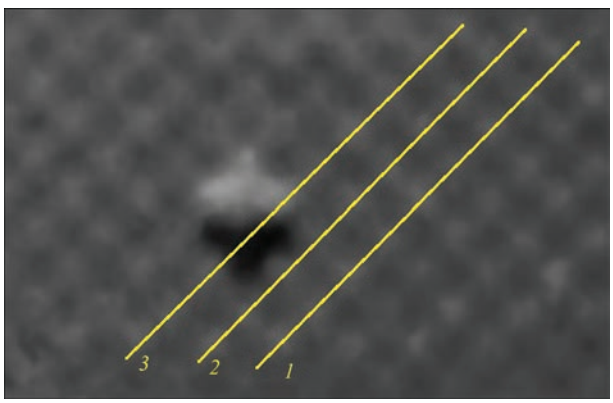


Figure 12. Graphical representation of the deformation of a panel surface with an internal defect under internal pressure loading

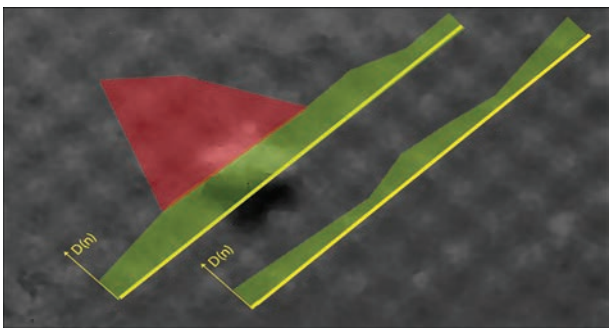


Figure 14. Graphical representation of the results of applying the algorithm for automatic defect localization

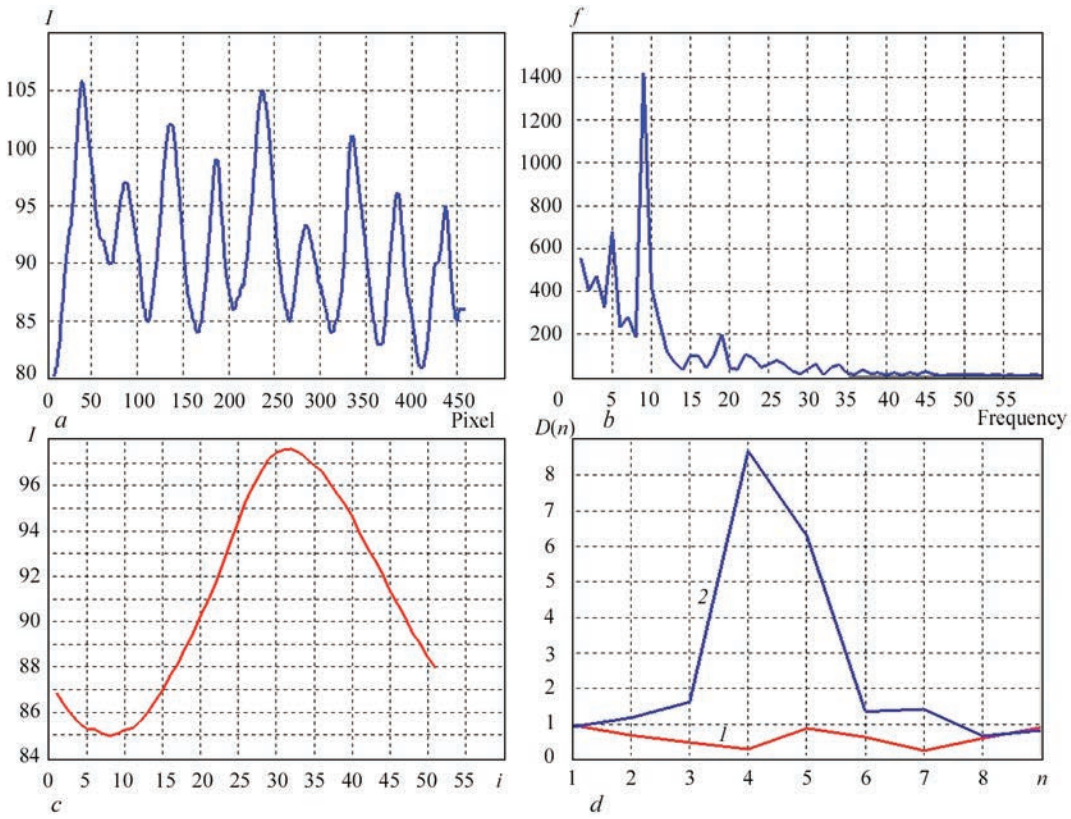


Figure 13. Determination of the location of a defective area based on shearography data: *a* — surface profile in cross-section *1*; *b* — Fourier spectrum of data along the profile; *c* — diagram of the dimensionless quantity *I* for the reference segment; *d* — diagrams of the function *D*(*n*)

area. A reference defect-free area was obtained by calculating the average values (Figure 13, *c*). A comparison was made between the reference defect-free area and the data along profiles 1 and 3, and the value of the function *D*(*n*) was calculated (Figure 13, *d*), where *n* is the segment number. For the defect-free profile (curve *1*), the amplitude of the function values is significantly smaller than for the defective one (curve *2*).

A comparison of the experimentally obtained deformation pattern of the panel (Figure 14) with the algorithm results showed that the function *D(n)*, which indicates the deviation of the deformation in the studied segments from the reference defect-free segment, ensures reliable defect localization.

The obtained results confirm the correctness of the proposed algorithm for processing shearography data and its effectiveness for the automated localization of defects in three-layer welded panels.

CONCLUSIONS

Mathematical simulation of the stress-strain state of a two-layer welded panel under thermal loading was performed using the finite element method. This made it possible to investigate the effect of defects on the deformation of structure surfaces. It was shown that using the displacement derivative $\partial w/\partial y$ makes it possible to detect defects more clearly than to analyzing displacements alone. This justifies the use of the shearography method for non-destructive testing of such structures.

Based on statistical data analysis and the application of Fourier analysis and differentiation techniques, an algorithm for the automated detection of defective areas during non-destructive testing using laser interferometry methods has been developed for the first time.

Studies have shown that the effectiveness of the method for locating defects is based on identifying the period of characteristic features, determining a reference segment, and calculating the function *D*(*n*), which reflects the degree of deviation in the deformation of the studied segment from the defect-free reference segment. It has been established that median filtering when used to form the reference profile yields more accurate results compared to simple averaging, resulting in lower values of the function *D*(*n*) in defect-free segments.

The proposed method for determining the location of defects has demonstrated high efficiency in analyzing data obtained from model and experimental studies of welded panels. The effectiveness of the algorithm for the automated detection of defective areas in metal multilayer thin-walled structures has been confirmed both on model data obtained under thermal loading and on experimental data from shearography testing of a panel of a different design under mechanical loading, which demonstrates the versatility of the

approach for a broad class of thin-walled structures with a periodic configuration.

ACKNOWLEDGMENTS

The study was conducted as part of Project 2025.07/0312 "Innovative Complex of AI-Enhanced Non-Contact Optical Diagnostics for Advanced Technological Components", funded by the National Research Foundation of Ukraine as part of the "Excellent Science In Ukraine 2026-2028" competition.

REFERENCES

1. Falchenko, Yu.V., Petrushynets, L.V. (2018) Modern methods of manufacturing three-layer panels of aluminium alloys (Review). *The Paton Welding J.*, **6**, 32–39. DOI: https://doi.org/10.15407/tpwj2018.06.05
2. Altenbach, H., Eremeyev, V. (2017) Thin-walled structural elements: Classification, classical and advanced theories, new applications. In: *Shell-like structures*, 1–62. DOI: https://doi.org/10.1007/978-3-319-42277-0_1
3. Ghaffari, B., Mozurkewich, G. (2010) Non-destructive evaluation of spot-weld quality. In: *Failure mechanisms of advanced welding processes, Woodhead publishing series in welding and other joining technologies*, 101–136. DOI: https://doi.org/10.1533/9781845699765.101
4. Le, M., Kim, J., Kim, S., Lee, J. (2016) Nondestructive testing of pitting corrosion cracks in rivet of multilayer structures. *Inter. J. Precis. Eng. Manuf.*, **17**, 1433–1442. DOI: https://doi.org/10.1007/s12541-016-0169-7
5. Le, M., Kim, J., Kim, S., Lee, J. (2018) B-scan ultrasonic testing of rivets in multilayer structures based on short-time Fourier transform analysis. *Measurement*, **128**, 495–503. DOI: https://doi.org/10.1016/j.measurement.2018.06.049
6. Soyturk, F., Günöz, A., Kara, M. (2023) Detection of welding defects by non-destructive testing methods. *Inter. Conf. on Applied Engineering and Natural Sciences*, 1(**1**), 424–427. DOI: https://doi.org/10.59287/icaens.1033
7. Thornton, M., Han, L., Shergold, M. (2012) Progress in NDT of resistance spot welding of aluminium using ultrasonic C-scan. *NDT & E International*, **48**, 30–38. DOI https://doi.org/10.1016/j.ndteint.2012.02.005
8. Yang, L., Chuai, R., Cai, G. et al. (2024) Ultrasonic non-destructive testing and evaluation of stainless-steel resistance spot welding based on spiral C-scan technique. *Sensors*, **24**, 4771. DOI: https://doi.org/10.3390/s24154771
9. Ulbrich, D., Psuj, G., Wypych, A. et al. (2023) Inspection of spot welded joints with the use of the ultrasonic surface wave. *Materials*, 16(**21**), 7029. DOI: https://doi.org/10.3390/ma16217029
10. Mathiszik, C., Koal, J., Schmale, H.C., Füssel, U. (2026) Non-destructive testing of resistance spot welds by magnetic evaluation. In: *Proc. of the 14th European Conf. on Non-Destructive Testing 2026 (ECNDT 2026), June 15–19, 2026, Verona, Italy*. DOI: https://doi.org/10.58286/33348
11. Hung, Y.Y., Ho, H.P. (2005) Shearography: An optical measurement technique and applications. *Mater. Sci. Eng.*, 49(**3**), 61–87. DOI: https://doi.org/10.1016/j.mser.2005.04.001
12. Xu, N., Xie, X., Harmon, G. et al. (2012) Quality inspection of spot welds using digital shearography. *SAE Inter. J. of Materials and Manufacturing*, 5(**1**), 96–101. DOI: https://doi.org/10.4271/2012-01-0182
13. Hung, Y.Y., Yang, L.X., Huang, Y.H. (2013) Non-destructive evaluation (NDE) of composites: Digital shearography. In: *Woodhead publishing series in composites science and engineering*, 84–115. DOI: https://doi.org/10.1533/9780857093554.1.84
14. Lobanov, L.M., Savitsky, V.V., Kyianets, I.V. et al. (2021) Non-destructive testing of elements of titanium honeycomb panels by shearography method using vacuum load. *The Paton Welding J.*, **12**, 49–54. DOI: https://doi.org/10.37434/tpwj2021.12.08
15. Stetsyuk, P.I., Savitsky, V.V. (2018) On defects search in regular 3D-structures. *J. of Automation and Information Sciences*, 50(**3**), 21–37. DOI: https://doi.org/10.1615/JAutomatInfScien.v50.i3.20
16. Ribes, A., Caremoli, C. (2007) SALOME platform component model for numerical simulation. In: *Proc. of the 31st Inter. Conf. on Annual Computer Software and Applications. (COMPSAC 2007)*, 553–564. DOI: https://doi.org/10.1109/COMPSAC.2007.185
17. Code_Aster: *Finite element analysis of structures and thermomechanics for studies and research. Électricité de France (EDF)*, 1989–2026. https://www.code-aster.org
18. Oppenheim, A.V., Schafer, R.W. (2009) *Discrete-time signal processing*. 3rd Ed. Upper Saddle River, Pearson.
19. Huang, T., Yang, G., Tang, G. (1979) A fast two-dimensional median filtering algorithm. *IEEE Transact. on Acoustics, Speech, and Signal Processing*, 27(**1**), 13–18. DOI: https://doi.org/10.1109/tassp.1979.1163188

ORCID

L.M. Lobanov: 0000-0001-9296-2335,
I.L. Shkurat: 0009-0003-1888-4203,
O.P. Shutkevych: 0000-0001-5758-2396,
I.V. Kyianets: 0000-0002-2559-8200,
V.V. Savitsky: 0000-0002-2615-1793

CONFLICT OF INTEREST

The Authors declare no conflict of interest

CORRESPONDING AUTHOR

I.L. Shkurat
E.O. Paton Electric Welding Institute of the NASU
11 Kazymyr Malevych Str., 03150, Kyiv, Ukraine
E-mail: innashkurat2909@gmail.com

SUGGESTED CITATION

L.M. Lobanov, I.L. Shkurat, O.P. Shutkevych, I.V. Kyianets, V.V. Savitsky (2026) Automated detection of defective areas in a multilayer thin-walled structure with a periodic configuration using laser interferometry methods.
The Paton Welding J., **10**, 3–11.
DOI: https://doi.org/10.37434/tpwj2026.10.01

JOURNAL HOME PAGE

https://patonpublishinghouse.com/eng/journals/tpwj

Received: 12.07.2026
Received in revised form: 20.08.2026
Accepted: 30.10.2026